



15 **Apparent efficiency of serially coupled columns in isocratic and gradient elution**  
16 **modes**

17  
18 **Abstract**

19 The goal of this work was to understand the variation of apparent efficiency when serially  
20 coupling columns with identical stationary phase chemistries, but with differences in their  
21 kinetic performance. For this purpose, a mathematical treatment was developed both for  
22 isocratic and gradient modes to assess the change in plate numbers and peak widths when  
23 coupling arbitrary several columns. To validate the theory, experiments were also carried out  
24 using various mixtures of compounds, on columns packed with different particle sizes, to  
25 mimic highly efficient (new, not used) and [poorly efficient columns \(used one with many](#)  
26 [injections\)](#). Excellent agreement was found between measured and calculated peak widths.  
27 [The average error in prediction was about 5 % \(which may be explained by the additional](#)  
28 [volume of the coupling tubes\).](#)

29 In isocratic mode, the plate numbers are not additive when the coupled columns possess  
30 different efficiencies, and a limiting plate count value can be calculated depending on the  
31 efficiency and length of the individual columns. [Theoretical efficiency limit can also be](#)  
32 [determined assuming one column in the row with infinite efficiency.](#)

33 In gradient [elution](#) mode, the columns' order has a role (non-symmetrical system). When the  
34 last column has high enough efficiency, the gradient band compression effect may  
35 outperform the competing band broadening caused by dispersive and diffusive processes  
36 [\(peak sharpening\)](#). Therefore, in gradient mode, the columns should generally be  
37 sequentially placed according to their increasing efficiency.

38  
39 **Keywords:**

40 Column coupling, apparent efficiency, plate number, peak capacity, column length

## 42 1. Introduction

43 The idea of coupling columns to analyze complex samples appeared quite early in  
44 chromatography [1,2,3,4,5,6]. The purpose of column coupling can be either to improve  
45 kinetic performance by increasing the column length or adjust selectivity by combining  
46 different stationary phase chemistries. This latter idea lead to the development of  
47 multidimensional chromatographic separations.

48 There are two ways to combine two or more columns in mono-dimensional separations,  
49 namely parallel and serial arrangements [7]. Serial columns generally outperform parallel  
50 setups, as the resolution power is appreciably extended in this configuration. The effect of  
51 changes in column length is different in the serial and parallel approaches. The serially  
52 coupled columns approach has an intrinsic advantage: there is an additional separation  
53 factor (the column length), which however has no consequence in the experimental effort. In  
54 practice, each serial combination of short columns of different chemical nature and length  
55 operates as a new column, with its own selectivity. This increases enormously the wealth of  
56 columns available in a laboratory, from which the best one can be selected for a given  
57 application [7].

58 In most cases, the aim of column coupling remains to increase the chromatographic  
59 performance. The kinetic plot method (KPM) is often used as a design tool to find out the  
60 optimal column length to achieve a given number of theoretical plates [8,9]. The KPM can be  
61 used to predict the analysis time and efficiency which vary over a wide range of different  
62 column lengths, from very short to very long columns. Although the length independence is  
63 implicitly contained in the definition of the plate height concept, there are a number of cases  
64 wherein deviations from this behavior can be expected (axial temperature gradient due to  
65 viscous heating, extra-column band broadening effects which have relatively higher impact  
66 on small columns, side-wall effects that persist along the column length, pressure-related  
67 effects, etc.) [10,11,12,13]. The possibility to predict the performance of coupled columns  
68 systems has been extensively studied in the past. Coupling of up to six columns (900 mm = 6  
69 x 150 mm) showed that the KPM prediction was in good agreement with the obtained

70 performance on the coupled column system [14]. In another study [15], it has been  
71 demonstrated that up to 8 columns (packed with 5  $\mu\text{m}$  particles) could be coupled in series  
72 and operated at a constant flow rate without any significant loss of efficiency, again implying  
73 that the observed plate heights were independent on the column length.

74 The best combination of coupled columns in isocratic mode having different lengths and  
75 particle sizes was determined in a previous study from Cabooter *et al.* based on the Knox-  
76 Saleem speed limit [16]. Considering an ultrahigh-performance liquid chromatography  
77 (UHPLC) system operating at a pressure of 1200 bar, the best possible serial connection  
78 system can approach the 75–85 % of its Knox-Saleem limit whereas a three-column parallel  
79 system can only get about 50–60 % of the speed limit, while needing 50–100 % more total  
80 column length. In absolute terms, the serially-connected system with individually optimized  
81 segment lengths should be able to cover a range of 5000–75,000 theoretical plates in an  
82 average analysis time of 14.3 min when using a 1200 bar instrument [16].

83 When working in gradient mode, the overall peak capacity can be predicted in a very similar  
84 way on the basis of peak capacity measured on one single column, and assuming no  
85 differences in the performance of columns that will be coupled in series. Peak capacity  
86 prediction has indeed shown very good accuracy when coupling four columns of 150 mm in  
87 series [17]. Despite neglecting the possible variations in performance of the individual  
88 columns (different batches, history of the column), the kinetic performance limit approach  
89 works well in practice, as long as chromatographers couple the same type of columns (same  
90 stationary phase and dimension) in series.

91 Therefore, in isocratic mode the plate numbers are expected to be additive, while in gradient  
92 mode, the peak capacity is proportional with the square root of the column length [18].

93 Serial column coupling can be useful for various types of applications and is particularly used  
94 in RPLC mode [19]. By using a 450 mm long column (3 x 150 mm), the peak capacity of an  
95 antibody peptide mapping analysis was increased up to  $n_c = 704$  [20]. The same concept has  
96 also been used for intact and sub-units antibody analysis [20]. Another study showed the  
97 possibilities to achieve high plate count and peak capacity at various combinations of column

98 lengths and temperatures [21]. Column coupling has also been applied in ion-exchange (IEX)  
99 chromatography to improve the separation of intact antibody charge-variants [22]. In  
100 supercritical fluid chromatography (SFC), 4 columns (4 x 100 mm) were successfully coupled  
101 to increase the separation of 24 pharmaceutical compounds [23]. Column coupling can also  
102 be applied for chiral separations [24]. As an example, an in-line coupling of achiral and chiral  
103 columns was shown to be a good alternative to multidimensional chiral chromatography [24].  
104 Coupling columns of different pore sizes in series is also commonly used in size exclusion  
105 chromatography (SEC) to tune the selectivity of polymer separations [25].

106 Other purposes of column coupling can be post-column derivatization, on-line clean-up or the  
107 protection of the analytical column by using guard (pre-) columns [26,27].

108 The purpose of this study was to estimate and measure the apparent efficiency of columns  
109 made of identical stationary phase chemistry but possessing differences in their kinetic  
110 performance. It may happen that the individual columns do not have identical efficiency  
111 (different batch, different lifetime and antecedents, or different packing quality which is well-  
112 known to be dependent on column length and diameter [28]). Different particle sizes were  
113 used to mimic columns of different batches or columns providing different efficiencies when  
114 coupling them in series. In isocratic mode, the plate numbers do not always seem additive  
115 and kinetic performance has a limiting value, depending on the efficiency and length of the  
116 individual columns. Furthermore, in gradient elution mode, the system is indifferent to the  
117 column order. Theory has been developed to show the evolution of plate numbers for  
118 coupling arbitrary several columns in isocratic mode and to predict peak widths for two  
119 columns system in gradient mode. Experimental measurements have been performed to  
120 validate the theory.

121

## 122 2. Theory

### 123 2.1 Peak widths in isocratic elution

124 The band dispersion in serially connected columns can be calculated by solving the following  
125 ordinary differential equation:

126 
$$\frac{d\sigma_z^2}{dz} = H(z) \quad (1)$$

127 where  $\sigma_z^2$  is the spatial variance of bands of compounds inside the column,  $z$  the spatial  
 128 variable, and  $H(z)$  the height equivalent to a theoretical plate, HETP.

129 
$$H(z) = H_i \quad \text{if} \quad \sum_{j=0}^{i-1} L_j \leq z < \sum_{j=1}^i L_j \quad (2)$$

130 where  $H_i$  and  $L_i$  are the HETP and length of the  $i^{\text{th}}$  column, respectively. Note that  $L_0$  is  
 131 equal to zero.

132 The solution of Eq. (1) in case of  $n$  sequentially connected columns with the initial condition  
 133  $\sigma_z^2(0) = 0$  is:

134 
$$\sigma_z^2 = \sum_{i=1}^n L_i H_i = \sum_{i=1}^n \frac{L_i^2}{N_i} \quad (3)$$

135 Assuming that retention factors ( $k$ ) of solutes are the same in all the columns (identical  
 136 stationary phase chemistry), the retention time of a compound can be expressed as:

137 
$$t_R = \sum_{i=1}^n t_{R,i} = (1+k) \sum_{i=1}^n t_{0,i} = (1+k) \sum_{i=1}^n \frac{L_i}{u_{0,i}} \quad (4)$$

138 where  $t_{0,i}$  is the hold-up time, and  $u_{0,i}$  is the [average linear velocity](#) of the eluent in the  $i^{\text{th}}$   
 139 column.

140 [By matching the spatial \( \$\sigma\_z\$ \) and time \( \$\sigma\$ \) variances through the definition of efficiency and](#)  
 141 [replacing  \$t\_R\$  by Eq. \(4\), the following is obtained for a chromatographic peak eluted from  \$n\$](#)   
 142 [sequentially connected columns is:](#)

143 
$$\sigma^2 = \sigma_z^2 \frac{(1+k)^2}{u_{0,n}^2} \quad (5)$$

144 The fraction on the right hand side of Eq. (5) can be expressed from Eq. (4) as:

145 
$$\frac{1+k}{u_{0,n}} = \frac{t_R}{L_n} \frac{V_{0,n}}{V_0} \quad (6)$$

146 where  $L_n$  and  $V_{0,n}$  are the length and dead volume of the last segment,  $V_0$  is the total dead  
 147 volume of the  $n$  sequentially connected columns. Explicitly,  $V_{0,i} = L_i \frac{d_i^2 \pi}{4} \varepsilon_i$  with  $d_i$  and  $\varepsilon_i$  are  
 148 the internal diameter and total porosity of column  $i$ .

149 Eq. (6) can be combined with Eq. (5) and the peak width can be calculated as:

$$150 \quad w = 4\sigma = 4\sqrt{\sum_{i=1}^n \frac{L_i^2 t_R V_{0,n}}{N_i L_n V_0}} = 4\alpha t_R \quad (7)$$

151 where,

$$152 \quad \alpha = \frac{1}{L_n} \sqrt{\sum_{i=1}^n \frac{L_i^2 V_{0,n}}{N_i V_0}} \quad (8)$$

153 The total plate number of the sequentially connected columns is the sum of the number of  
154 theoretical plates of the  $n$  columns. The apparent plate number, however, can be calculated  
155 as:

$$156 \quad N_{app} = \frac{t_R^2}{\sigma^2} = \frac{1}{\alpha^2} \quad (9)$$

157 Eqs. (8) and (9) can be generalized after the following considerations:

$$158 \quad \lambda_i = \frac{L_i}{L_n}, \quad v_i = \frac{N_i}{N_n}, \quad \omega_i = \frac{V_{0,i}}{V_{0,n}} \quad (10)$$

159 Accordingly,

$$160 \quad \alpha = \frac{1}{\sqrt{N_n}} \sqrt{1 + \sum_{i=1}^{n-1} \frac{\lambda_i^2}{v_i} \frac{1}{1 + \sum_{i=1}^{n-1} \omega_i}} \quad (11)$$

161 and,

$$162 \quad N_{app} = N_n \frac{(1 + \sum_{i=1}^{n-1} \omega_i)^2}{1 + \sum_{i=1}^{n-1} \frac{\lambda_i^2}{v_i}} \quad (12)$$

163 The ratio of  $N_{app}$  and the total plate number is:

$$164 \quad \frac{N_{app}}{\sum_{i=1}^n N_i} = \frac{(1 + \sum_{i=1}^{n-1} \omega_i)^2}{(1 + \sum_{i=1}^{n-1} v_i) \left(1 + \sum_{i=1}^{n-1} \frac{\lambda_i^2}{v_i}\right)} \quad (13)$$

165 For a two-column system Eqs. (11), (12) and (13) become:

$$166 \quad \alpha = \frac{1}{\sqrt{N_2}} \sqrt{1 + \frac{\lambda_1^2}{v_1} \frac{1}{1 + \omega_1}} \quad (14)$$

$$167 \quad N_{app} = N_2 \frac{(1 + \omega_1)^2}{1 + \frac{\lambda_1^2}{v_1}} \quad (15)$$

$$168 \quad \frac{N_{app}}{N_1 + N_2} = \frac{(1 + \omega_1)^2}{(1 + v_1) \left(1 + \frac{\lambda_1^2}{v_1}\right)} \quad (16)$$

169 There are also several specific situations for two-columns:

170 If the plate numbers of the two columns are equal:

$$171 \quad N_{app} = \frac{N}{1 + \frac{L_1^2}{L_2^2}} \left( 1 + \frac{V_{0,1}}{V_{0,2}} \right)^2 \quad (17)$$

172 If the column diameters are equal:

$$173 \quad N_{app} = \frac{N_1 N_2}{N_1 + \frac{L_1^2}{L_2^2} N_2} \left( 1 + \frac{L_1}{L_2} \right)^2 \quad (18)$$

174 If the column diameters and lengths are equal:

$$175 \quad N_{app} = 4 \frac{N_1 N_2}{N_1 + N_2} \quad (19)$$

176 If the plate numbers and diameters of the two columns are equal:

$$177 \quad N_{app} = N \frac{(L_1 + L_2)^2}{L_1^2 + L_2^2} \quad (20)$$

178 If the efficiency of one of the two columns is infinite ( $N_2 = \infty$ )

$$179 \quad N_{app} = N_1 \frac{L_2^2}{L_1^2} \left( 1 + \frac{V_{0,1}}{V_{0,2}} \right)^2 \quad (21)$$

180 If the efficiency of one of the two columns is infinite ( $N_2 = \infty$ ) and the column dimensions are

181 identical:

$$182 \quad N_{app} = 4N_1 \quad (22)$$

183 Peak capacity,  $n$ , can be obtained as the solution of the following ordinary differential

184 equation with the initial condition of  $n(t_1) = 1$ :

$$185 \quad \frac{dn}{dt} = \frac{1}{w} \quad (23)$$

186 where  $w$  is peak width as a function of time,  $t$ .

187 The peak capacity of a series of columns connected together in isocratic mode can then be

188 calculated as the solution of Eq. (23):

$$189 \quad n = 1 + \frac{1}{4\alpha} \ln \frac{t_n}{t_1} = 1 + \frac{\sqrt{N_{app}}}{4} \ln \frac{t_n}{t_1} \quad (24)$$

190 For a two-columns system, the following equation can be written:

191 
$$n = 1 + \frac{1}{4} \sqrt{\frac{N_1 N_2}{N_1 + \frac{L_1^2}{L_2^2} N_2}} \left( 1 + \frac{V_{0,1}}{V_{0,2}} \right) \ln \frac{t_n}{t_1} \quad (25)$$

192 If the column dimensions are identical and one of the columns has an infinite efficiency ( $N_2 =$   
 193  $\infty$ ):

194 
$$n = 1 + \frac{\sqrt{N}}{2} \ln \frac{t_n}{t_1} \quad (26)$$

195

## 196 2.2 Peak widths in gradient elution

197 In gradient chromatography, the arrival time of a peak to a position  $z$  along the column is no  
 198 longer just proportional to time, but has to be retrieved from solving a differential equation,  
 199 given by:

200 
$$\frac{dt}{dz} = \frac{1}{u}, \quad t(0) = 0 \quad (27)$$

201 where the velocity  $u$  is given by the [instantaneous linear velocity of the solute, related to that](#)  
 202 [of the mobile phase \( \$u\_0\$ \) through the solute retention \( \$k\$ \):](#)

203 
$$u = \frac{u_0}{1+k} \quad (28)$$

204 [Notice that the condition  \$t\(0\) = 0\$  implies a negligible dwell volume. This is always the case](#)  
 205 [for initially highly retained compounds, that are stopped at the head of the column until the](#)  
 206 [gradient releases them.](#) According to the linear solvent strength (LSS) theory, the retention  
 207 factor can be written as a function of the mobile phase composition [\[29\]](#):

208 
$$k = k_w e^{-S\phi} \quad (29)$$

209 where  $S$  is the slope of the LSS model (log  $k$  vs. % organic modifier) and  $k_w$  is the  
 210 extrapolated value of  $k$  for a compound eluted with pure A eluent (i.e.,  $\Phi=0$ ). When running a  
 211 linear gradient [over a time  \$t\_G\$](#)  the mobile phase composition [at the inlet of the column](#) is given  
 212 by:

213 
$$\phi = \phi_0 + \frac{t}{t_G} \Delta\phi \quad (30)$$

214 The retention at a time  $t$  and position  $z$ , [taking into account the time  \$z t\_0/L\$  it takes for the](#)  
 215 [mobile phase to reach that point,](#) will be ([again neglecting the dwell volume](#)):

216 
$$k = k_0 \exp \left\{ -b \left( \frac{t}{t_0} - \frac{z}{L} \right) \right\} \quad (31)$$

217 where  $k_0 = k_w e^{-S\phi_0}$  is the initial retention,  $L$  the length of the column,  $t_0 = L/u_0$  the hold-up  
 218 time, and:

219 
$$b = S\Delta\phi \frac{t_0}{t_G} \quad (32)$$

220 Is the intrinsic gradient steepness.

221 The solution of (27) is the well-known chromatography formula:

222 
$$t(z) = t_0 \left[ \frac{z}{L} + \frac{1}{b} \ln \left( 1 + k_0 b \frac{z}{L} \right) \right] \quad (33)$$

223 The time to travel to  $z = L$  is the retention time, expressed as:

224 
$$t_R = t(L) = t_0 \left[ 1 + \frac{1}{b} \ln(1 + k_0 b) \right] \quad (34)$$

225 Peak width is mostly affected by diffusion and dispersion processes and by the gradient band  
 226 compression effect. The peak is compressed because of the changes to its trajectory while  
 227 crossing the gradient within the column. During gradient elution, the rear part of the peak  
 228 moves faster than its front part, because the mobile phase strength increases along the  
 229 column. The steeper the gradient, the higher the band compression effect is. To model the  
 230 band compression effect, it is useful to consider a peak between a point  $z$  and  $\tilde{z} = z + \sigma_z$ .

231 Then the next formula can be written:

232 
$$\frac{d\sigma_z}{dt} = \frac{d\tilde{z}}{dt} - \frac{dz}{dt} = u(\tilde{z}, t) - u(z, t) = u(z + \sigma_z, t) - u(z, t) \quad (35)$$

233 When  $w$  is small compared to the total length over which the motion of the peak is integrated,  
 234 the right-hand side of eq (35) can be expanded at first order in  $w$  to obtain:

235 
$$\frac{d\sigma_z}{dt} = \partial_z u(z, t) \cdot \sigma_z \quad (36)$$

236 Our goal is to have  $z$  as an independent variable, so with the chain rule, the following  
 237 equation can be obtained:

238 
$$\frac{d\sigma_z}{dz} = \frac{d\sigma_z}{dt} \frac{dt}{dz} = \frac{\partial_z u}{u} \sigma_z = \partial_z \ln u \cdot \sigma_z \quad (37)$$

239 The speed gradient at a given position is obtained by plugging in the solution the equation  
 240 (33):

241 
$$\partial_z \log u (z, t(z)) = \frac{-1}{L} \frac{p}{1+\frac{pz}{L}} \quad (38)$$

242 where,

243 
$$p = b \frac{k_0}{1+k_0} \quad (39)$$

244 is a measure of the gradient steepness. It takes into account that initially unretained  
245 substances ( $k_0 = 0$ ) will not be compressed at all.

246 The band broadening effects can be dependent on the column HETP measured in isocratic  
247 mode, which we call here  $H_0$ ,

248 
$$\frac{d\sigma_z^2}{dz} = H_0 \quad (40)$$

249 Equation (40) can be joined with (37) to give:

250 
$$\frac{d\sigma_z^2}{dz} = H_0 + 2\partial_z \log u \cdot \sigma_z^2 \quad (41)$$

251 If the width  $\sigma_{z,0}^2$  at a given point along the column  $z_0$  (this will be necessary for the coupling)  
252 is known:

253 
$$\sigma_z^2(z_0) = \sigma_{z,0}^2 \quad (42)$$

254 the solution is:

255 
$$\sigma_z^2(z) = \frac{\sigma_{z,0}^2 \left(1 + \frac{pz_0}{L}\right)^2 + H_0(z-z_0) \left(1 + \frac{p(z+z_0)}{L} + \frac{1}{3} \frac{p^2(z^2+zz_0+z_0^2)}{L^2}\right)}{\left(1 + \frac{pz}{L}\right)^2} \quad (42)$$

256 By neglecting the initial peak width caused by the injection process,  $\sigma_{z,0}^2 = 0$  when  $z = 0$ , we  
257 obtain the known formula at elution ( $z = L$ ):

258 
$$\sigma_z^2(L) = H_0 L \frac{1+p+\frac{1}{3}p^2}{(1+p)^2} \quad (43)$$

259 We now assume a two-column system possessing different HETP values,  $H_1$  for length  $L_1$ ,  
260 and  $H_2$  for length  $L_2$ . If the same gradient steepness and linear velocity are considered on the  
261 two columns, then the migration can still be described by equation (33), with  $L = L_1 + L_2$ . In  
262 the first column, the width evolves from the injection width  $\sigma_{z,i}$  at  $z = 0$ . By setting  $H_0 = H_1$ ,  
263  $\sigma_{z,0} = \sigma_{z,i}$  and  $z_0 = 0$  in equation (42), the following equation can be obtained:

264 
$$\sigma_{z,1}^2(z) = \frac{\sigma_{z,i+H_1}^2 \left(1 + \frac{pz}{L} + \frac{1}{3} \left(\frac{pz}{L}\right)^2\right)}{\left(1 + \frac{pz}{L}\right)^2} \quad (44)$$

265 When it reaches  $z = L_1$ , it starts migrating under  $H_2$ . The coupling condition is:

266 
$$\sigma_{z,2}^2(L_1) = \sigma_{z,1}^2(L_1) \quad (45)$$

267 This means that  $\sigma_{z,2}$  follows equation (42), with  $H_0 = H_2$ ,  $z_0 = L_1$  and  $\sigma_{z,0}^2 = \sigma_{z,1}^2(L_1)$ , thus  
 268 defining:

269 
$$\theta = \frac{(H_1 - H_2)}{H_2} = \frac{H_1}{H_2} - 1 \quad (46)$$

270 the solution becomes:

271 
$$\sigma_{z,2}^2(z) = \frac{\sigma_{z,i+H_2}^2 \left[ \left(1 + \frac{L_1}{z}\theta\right) + \frac{pz}{L} \left(1 + \left(\frac{L_1}{z}\right)^2 \theta\right) + \frac{1}{3} \left(\frac{pz}{L}\right)^2 \left(1 + \left(\frac{L_1}{z}\right)^3 \theta\right) \right]}{\left(1 + \frac{pz}{L}\right)^2} \quad (47)$$

272 or over the whole coupled system:

273 
$$\sigma_z(z) = \begin{cases} \sigma_{z,1}(z) & \text{if } 0 \leq z \leq L_1 \\ \sigma_{z,2}(z) & \text{if } L_1 \leq z \leq L \end{cases} \quad (48)$$

274 The result is very similar to (44), with a correction factor proportional to  $\theta$ . At elution,  $z = L =$

275  $L_1 + L_2$ :

276 
$$\sigma_{z,e}^2 = \sigma_{z,2}^2(L) = \frac{\sigma_{z,i+H_2}^2 \left[ \left(1 + \frac{L_1}{L}\theta\right) + p \left(1 + \left(\frac{L_1}{L}\right)^2 \theta\right) + \frac{1}{3} p^2 \left(1 + \left(\frac{L_1}{L}\right)^3 \theta\right) \right]}{(1+p)^2} \quad (49)$$

277 Please note that the dependence in  $H_1$  only comes through  $\theta$ . In particular, if  $L_1$  is smaller

278 than  $L$ , then the efficiency is basically dominated by the second column.

279

### 280 3. Experimental

#### 281 3.1 Chemicals and columns

282 Acetonitrile, methanol and ethanol (gradient grade) were purchased from Sigma-Aldrich  
 283 (Buchs, Switzerland). Water was obtained with a Milli-Q Purification System from Millipore  
 284 (Bedford, MA, USA).

285 Uracil, methylparaben, ethylparaben, propylparaben, butylparaben, cannabidivarin (CBDV),  
 286 cannabigerolic acid (CBGA), tetrahydrocannabivarin (THCV), cannabichromene (CBC),  
 287 delta9-tetrahydrocannabinolic acid (THCA-A) and human serum albumin (HSA), were

288 purchased from Sigma–Aldrich. Cannabidiolic acid (CBDA), cannabigerol (CBG), cannabidiol  
289 (CBD), cannabinal (CBN), (-)-delta9-THC (d9-THC) and (-)-delta8-THC (d8-THC) were  
290 purchased from Lipomed AG (Arlesheim, Switzerland).

291 Ammonium hydroxide solution, formic acid (FA), trifluoroacetic acid (TFA), dithiothreitol  
292 (DTT) and trypsin were obtained from Sigma-Aldrich.

293 X-Bridge C18 (5  $\mu\text{m}$ , 150 x 4.6 mm) (A), X-Bridge C18 (3.5  $\mu\text{m}$ , 100 x 4.6 mm) (B) and X-  
294 Bridge C18 (2.5  $\mu\text{m}$ , 75 x 4.6 mm) (C) columns were purchased from Waters (Milford, MA,  
295 USA). Jupiter C18 (5  $\mu\text{m}$  300 Å, 150 x 2.0 mm) (D) and Jupiter C18 (3  $\mu\text{m}$  300 Å, 150 x 2.0  
296 mm) (E) columns were purchased from Phenomenex (Torrance, CA, USA).

297

### 298 3.2 Equipment and software

299 The measurements were performed using a Waters Acquity UPLC™ I-Class system  
300 equipped with a binary solvent delivery pump, an autosampler and UV detector and/or  
301 fluorescence detector (FL). The system includes a flow through needle (FTN) injection  
302 system equipped with 15  $\mu\text{L}$  needle, a 0.5  $\mu\text{L}$  UV flow-cell and a 2  $\mu\text{L}$  FL flowcell. The  
303 connection tube between the injector and column inlet was 0.003" I.D. and 200 mm long  
304 (active preheating included), and the capillary located between the column and detector was  
305 0.004" I.D. and 200 mm long. The overall extra-column volume ( $V_{\text{ext}}$ ) was about 8.5  $\mu\text{L}$  and  
306 11  $\mu\text{L}$  as measured from the injection seat of the auto-sampler to the detector cell (UV and  
307 FL, respectively). The average extra-column peak variance of our system was found to be  
308 around  $\sigma_{EC}^2 \sim 0.5 - 3 \mu\text{L}^2$  (depending on the flow rate, injected volume, mobile phase  
309 composition and solute). Data acquisition and instrument control were performed by  
310 Empower Pro 3 Software (Waters).

311

### 312 3.3 Chromatographic conditions and sample preparation

#### 313 3.3.1. Apparent plate numbers: Isocratic measurements of parabens and uracil

314 A mix solution containing uracil, methylparaben, ethylparaben, propylparaben and  
315 butylparaben was prepared in 80 : 20 v/v water : acetonitrile at 50 µg/mL.

316 For isocratic chromatographic measurements, the mobile phase was composed of 55 : 45 v/v  
317 water : acetonitrile. Experiments were performed at a flow rate of 1 mL/min at ambient  
318 temperature. Detection was carried out at 254 nm (40 Hz), the injection volume was 5 µL.  
319 The plate numbers were measured on three single columns, namely the 5 µm, 150 x 4.6 mm  
320 (A), 3.5 µm, 100 x 4.6 mm (B) and 2.5 µm, 75 x 4.6 mm (C) columns, then the columns were  
321 coupled in series using 5 cm long (0.175 mm ID) stainless steel tubing and the apparent  
322 plate numbers were measured. The following combinations were tested: (1) columns A + B,  
323 (2) columns A + C, (3) columns B + C and (4) columns A + B + C.

324

325 3.3.2. Apparent peak widths: gradient measurements of small molecules (mix of  
326 cannabinoids)

327 A mix solution containing eleven cannabinoids (i.e. CBDV, CBGA, THCV, CBC, THCA-A,  
328 CBDA, CBG, CBD, CBN, d9-THC and d8-THC) was prepared from individual stock solutions  
329 diluted in solvent having the same composition as the initial mobile phase (55 : 45 v/v 10 mM  
330 ammonium-acetate : acetonitrile) at 90 µg/mL. The individual stock solutions were prepared  
331 in either methanol, acetonitrile or ethanol depending on their solubility. Mobile phase “A” was  
332 10 mM ammonium-acetate (pH = 5.8), mobile phase “B” was acetonitrile. Linear gradients  
333 were run from 45 %B to 100 %B at 1 mL/min flow rate and ambient temperature. The  
334 gradient time ( $t_G$ ) over column length (L) ratio was kept constant ( $t_G/L=1$  min/cm) when  
335 running gradients on different column lengths (corresponds to e.g.  $t_G = 10$  min on 10 cm long  
336 column). Detection was carried out at 220 and 254 nm (40 Hz), the injection volume was 10  
337 µL. The peak widths (peak capacity) were measured on three single columns, namely on the  
338 5 µm, 150 x 4.6 mm (A), 3.5 µm, 100 x 4.6 mm (B) and 2.5 µm, 75 x 4.6 mm (C) columns,  
339 and then these columns were coupled in series using 5 cm long (0.175 mm ID) stainless  
340 steel tubing, and the apparent peak widths (peak capacity) were measured. The following

341 combinations were used: (1) columns A + B, (2) columns A + C, (3) columns B + C and (4)  
342 columns A + B + C.

343

344 3.3.3. Apparent peak widths: gradient measurements of peptides (HSA tryptic digest)

345 Tryptic digestion of human serum albumin (HSA) was carried out as described in a recent  
346 protocol [30]. Mobile phase "A" was 0.1 % TFA in water, mobile phase "B" was 0.1 % TFA in  
347 acetonitrile. Linear gradients were run from 10 to 70 %B at a flow rate of 0.3 mL/min and 50  
348 °C. The gradient time ( $t_G$ ) over column length (L) ratio was kept constant ( $t_G/L=2$  min/cm)  
349 when running gradients on different column lengths (corresponds to e.g.  $t_G = 30$  min on 15  
350 cm long column). Fluorescence detection was carried out at 280 nm as excitation and 350  
351 nm as emission wavelengths, the injection volume was 5  $\mu$ L. The peak widths (peak  
352 capacity) were measured on two widepore columns of 5  $\mu$ m, 150 x 2.0 mm (D) and 3  $\mu$ m,  
353 150 x 2.0 mm (E) columns, then these two columns were coupled in series using 5 cm long  
354 (0.175 mm ID) stainless steel tubing, and the apparent peak widths (peak capacity) were  
355 measured. The following combinations were used: (1) columns D + E and (2) columns E + D.

356

## 357 4. Results and Discussion

358 4.1. Apparent plate number in isocratic mode for serially coupled columns

359 As it is possible to couple together two columns possessing different lengths and efficiencies,  
360 an informative representation of the apparent plate number ( $N_{app}$ ) can be obtained when  
361 plotting the ratio of  $N_{app}/N_{sum}$  (where  $N_{sum}$  is the sum of the individual plate counts) as a  
362 function of  $N_1/N_2$  (corresponding to the efficiency of the first and second columns,  
363 respectively). In this type of representation, various ratios of column lengths ( $L_1/L_2$ ) can be  
364 tested. Figure 1 shows some plots for  $L_1/L_2 = 0.75, 1, 1.5$  and 2 (calculations are based on  
365 eq 18). As suggested by the theory, all the curves show a maxima ( $N_{app}/N_{sum} = 1$ ), indicating  
366 that the highest reachable efficiency with two serially coupled columns is equal to the sum of  
367 the individual plate numbers. However, it only occurs at a given ratio of column lengths.  
368 When coupling two columns of identical lengths ( $L_1/L_2 = 1$ ) in series, then this maximum

369 occurs when the columns possess identical plate numbers ( $N_1/N_2 = 1$ ). When the first column  
370 is twice longer than the second one ( $L_1/L_2 = 2$ ), then the maximum plate number is attained  
371 when the first column performs twice as high plate numbers than the second one ( $N_1/N_2 = 2$ ).  
372 Similarly, when  $L_1/L_2 = 1.5$  and  $0.75$ , the maximum performance is expected for  $N_1/N_2 = 1.5$   
373 and  $0.75$ , respectively. Accordingly, to obtain the maximum efficiency from equal coupled  
374 columns configuration, it is required that their plate heights should be the same. In this case,  
375 the apparent plate count is the sum of the individual plate counts. In any other case,  
376  $N_{app}/N_{sum}$  will be smaller than 1. An important feature of the system is its symmetric property,  
377 meaning that the system (or  $N$ ) is indifferent to the order. One can choose the more efficient  
378 column either in the first or the second position, without affecting the global efficiency.

379 **Table 1** shows the measured and calculated plate numbers on single columns (A, B and C)  
380 and serially coupled configurations (including two and three columns) for four model  
381 compounds (parabens). As shown, the measured and predicted plate numbers are in very  
382 good agreement, with a variation between measured and predicted efficiency comprised  
383 between -7 and +5 %. **Figure 1** also includes the experimentally measured values which fit  
384 quite well with the theoretical curves. As an example, **Figure 2** shows some representative  
385 chromatograms of the four parabens separated on three different columns with different  
386 lengths and efficiency as well as with the three columns serially coupled.

387 Another interesting aspect is to track the efficiency increase of two serially coupled columns  
388 compared to just one of the columns used for this coupling. **Figure 3** illustrates  $N_{app}/N_1$  as a  
389 function of  $N_1/N_2$  for three cases, namely for  $L_1/L_2 = 0.2$ , 1 and 2 with identical column  
390 diameters. When  $L_1/L_2 = 2$  (the first column is twice as long as the second one), the intercept  
391 of the curve corresponds to  $N_{app}/N_1 = 2.25$ . This means that the maximum efficiency is 2.25  
392 times higher vs. that of the first column. It occurs when the second column has infinite  
393 efficiency (intercept at  $N_1/N_2=0$ ). In this case, the second column only increases retention  
394 times without any effect on band broadening. As illustrated in **Figure 3**, it is not possible to  
395 attain higher plate numbers with this setup. On the other hand, if the efficiency of the second  
396 column is five times lower than that of the first column, then the apparent plate number of

397 serially coupled columns will be the same as of the first column. When  $N_1/N_2$  is above 5, the  
 398 overall efficiency of the coupled system is lower than the efficiency of the first column. This  
 399 means that it is possible to combine two HPLC columns that finally generate lower resolution  
 400 than that offered by the most efficient column alone. This counter instinctive consequence is  
 401 analogous to the band broadening effect due to the extra column contributions. Similarly,  
 402 when  $L_1/L_2 = 1$ , the maximum achievable efficiency is four times higher than that of the first  
 403 column, while if the efficiency of the second column is at least three times lower than the first  
 404 column, then no increase in efficiency is obtained when coupling these two columns. Finally,  
 405 when the first column is very short compared to the second column ( $L_1/L_2 = 0.2$ ) and the  
 406 second column has very high efficiency (infinite) then  $N_{app}/N_1 = 36$  can be attained when  
 407 coupling the columns.

408 In general, when efficiency of the second column is infinite, the apparent plate number of the  
 409 two-column system becomes:

$$410 \quad N_{app} = N_1 \left( \frac{1+\lambda}{\lambda} \right)^2 \quad (50)$$

411 The condition when additional gain of efficiency can be obtained by coupling two columns is:

$$412 \quad \nu < 1 + 2\lambda \quad (51)$$

413 or similarly,

$$414 \quad \xi > \frac{\lambda}{1+2\lambda} \quad (52)$$

415 where  $\nu = N_1/N_2$ ,  $\lambda = L_1/L_2$ , and  $\xi = H_1/H_2$ .

416 Accordingly, additional gain of efficiency and resolution is possible by coupling two HPLC  
 417 columns only if the column plate heights do not differ too significantly.

418

419 4.2. The evolution of peak width and peak capacity in gradient mode for serially coupled  
 420 columns

421 In gradient elution mode, the order of the columns is concerned, and the observed apparent  
 422 efficiency strongly depends on the order of the columns (non-symmetrical system). An  
 423 illustration is given in **Figure 4**. Assuming two columns (with the same internal diameter) with

424 plate heights,  $H = 10 \mu\text{m}$  and  $H = 40 \mu\text{m}$ , respectively coupled in series. The peak width will  
425 evolve in different ways depending on the column order and length of the individual  
426 segments (the different plate heights were assumed to mimic columns of different batches or  
427 the combination of old and new columns). The continuous lines in **Figure 4** show the peak  
428 widths for coupled columns possessing different efficiencies as a function of the position of  
429 the solute ( $z$ ) along its travel. The dashed lines correspond to columns having either  $H = 10$   
430  $\mu\text{m}$  or  $H = 40 \mu\text{m}$  efficiency along its entire length (10 cm) – as reference values.

431 **Figure 4A** shows the case where two segments of 5 cm are coupled at a moderate gradient  
432 steepness ( $p=1$ ). When placing the more efficient column in the first position and the less  
433 efficient one in the second position (continuous red line) – as expected – the peak will  
434 broaden drastically after entering the second (less efficient) column as the band broadening  
435 caused by dispersion and diffusion processes becomes more important. However, when  
436 having the less performing column in the first position and the most efficient column in the  
437 second position (continuous blue line), interestingly the peak width will decrease  
438 continuously during the travel of the solute along the second column (“peak sharpening”). It  
439 suggests that the gradient band compression effect outperforms the dispersive and diffusive  
440 effects in the second column as the more efficient column offers much lower  $H$  value than the  
441 first column. If the second - more efficient - column is very long compared to the first one, the  
442 peak width will approach the limiting value theoretically obtained only with the more efficient  
443 column - indeed, the dashed line (single column with maximal efficiency) is an asymptote of  
444 the solid line (coupled system), that are equal in the large  $z$  limit.

445 **Figure 4B** represents a situation where the column lengths are different. The first one is four  
446 times shorter than the second one. When placing the better column in the first position, then  
447 a trend similar to that of **Figure 4A** can be seen. However the coupled system approaches  
448 faster its limit (see the dashed and continuous red lines) because at the beginning of the  
449 solute’s travel along the column, the gradient compression effect is stronger than later during  
450 the travel (e.q. 38). When putting the more efficient column as the second one, then no band  
451 broadening occurs in the second column, and the peak width remains more or less constant

452 whilst the solute is traveling through the second column (continuous blue line). It suggests  
453 that the gradient band compression effect nearly compensates the band broadening caused  
454 by dispersion and diffusion processes. Please note that the differences between the coupled  
455 systems – with columns possessing different efficiencies - were larger in this case compared  
456 to the situation where the lengths were identical (see the differences at  $z = 10$  cm between  
457 the continuous blue and red lines in Figures 4A and 4B).

458 Finally, figure 4C corresponds to a situation with two columns of 5 cm – similarly to Figure 4A  
459 – but for a steeper gradient ( $p = 10$ ). The trends were similar as the ones observed in Figure  
460 4A, but as expected the gradient focusing effect was more important, and therefore the total  
461 peak width was smaller. When placing the better column in the second position (continuous  
462 blue line), the speed of peak compression was faster on the second column compared to the  
463 case where a flatter gradient was applied.

464 To verify the theory developed for predicting the peak width in gradient mode, two sets of  
465 compounds were analyzed using serially connected columns having different particle sizes  
466 and lengths. Figure 5 shows the separations of 11 cannabinoids on three different individual  
467 columns and on different combinations of two or three columns, as selected examples. Table  
468 1 contains the experimentally measured and predicted peak widths for the first and last  
469 eluting peaks. The peak width prediction for serially coupled columns was based on the peak  
470 widths measured on the individual columns. In particular, values for single column  
471 efficiencies were retrieved from direct measurements of peak width. These efficiencies were  
472 then used as the input for the coupled formula (e.q. 49). The measured and calculated widths  
473 were in very good agreement, as the average error in prediction was about 5-6 %.

474 Another experimental verification was performed by injecting HSA tryptic digest on two  
475 individual widepore columns packed with 5 and 3  $\mu\text{m}$  particles and on the combination of  
476 these two columns in different orders (Figure 6). Larger molecules (peptides) possess higher  
477  $S$  values, therefore it was interesting to check the validity of the model calculations for such  
478 molecules. The peak widths of the three most intense (and well separated) peaks was  
479 predicted for the coupled systems from the widths on the single columns. Again, very good

480 agreement was found between experimentally observed and calculated peak widths (Table  
481 3), as the average error in prediction was about 6 %. The results confirm the importance of  
482 the columns order as the order “D + E” always gave thinner peaks than “E + D” (both for  
483 predicted and measured peak widths).

484

## 485 **5. Conclusions**

486 The serially coupled columns approach has an intrinsic advantage as it offers an additional  
487 separation factor (the column length). In most cases, the column length is increased by  
488 coupling columns packed with the same material (i.e. stationary phase and particle size). In  
489 this case, the plate number observed with the coupled column system is the sum of the plate  
490 counts observed on the individual column segments. However, it may happen that the  
491 individual columns do not have identical efficiency (different batch, different lifetime and  
492 antecedents, or different packing quality which is well-known to be dependent on column  
493 length and diameter). Therefore, coupling columns with different efficiencies in series raises  
494 some questions: (1) What will be the final apparent efficiency?, (2) What is the maximum  
495 efficiency that can be reached?, and (3) Does the column order play a significant role?

496 Theory was developed for both isocratic and gradient modes, to predict the peak widths for  
497 coupled column systems. In isocratic mode, the plate numbers are not additive anymore  
498 when the columns possess different plate count, and kinetic performance has a limiting value  
499 which depends on the efficiency and length of the individual columns.

500 Furthermore, in gradient elution mode, the order of the columns is not indifferent. Indeed, the  
501 observed apparent efficiency significantly depends on the column order (non-symmetrical  
502 system). In combinations, when the latter column has higher efficiency, a decrease of the  
503 peak width is predicted (“peak sharpening”), when the solute travels this segment. This  
504 means that the gradient band compression effect compensates and outperforms the  
505 competing band broadening caused by dispersive and diffusive processes. Therefore, the  
506 columns should be placed in order of increasing efficiency.

507 Experimental measurements have been performed in both isocratic and gradient modes to  
508 verify the developed theory. Very good agreement was found between measured and  
509 calculated peak widths.

510 To conclude for serially coupled column systems in gradient mode, besides the total length of  
511 the coupled column, additional important factors are the order and lengths of the individual  
512 segments which must be considered when optimizing a gradient separation.

513

## 514 **6. Acknowledgements**

515 The authors wish to thank Jean-Luc Veuthey and Balazs Bobaly from the University of  
516 Geneva for fruitful discussions.

517 Davy Guillarme wishes to thank the Swiss National Science Foundation for support through a  
518 fellowship to Szabolcs Fekete (31003A 159494).

519 Krisztián Horváth acknowledges the financial support of the Hungarian Government and the  
520 European Union, with the co-funding of the European Social Fund in the frame of GINOP  
521 Programme [Code No: GINOP-2.3.2-15-2016-00016], and of the János Bolyai Research  
522 Scholarship of the Hungarian Academy of Sciences.

523 **References**

- 524 [1] J.L. Glajch, J.C. Gluckman, J.G. Charikofsky, J.M. Minor, J.J. Kirkland, Simultaneous  
525 selectivity optimization of mobile and stationary phases in RPLC for isocratic separations of  
526 phenylthiohydantoin amino acid derivatives, *J. Chromatogr.* 318 (1985) 23–39.
- 527 [2] P.H. Lukulay, V.L. McGuffin, Solvent modulation in liquid chromatography: extension to  
528 serially coupled columns, *J. Chromatogr. A* 691 (1995) 171–185.
- 529 [3] F. Garay, Application of a flow-tunable, serially coupled gas chromatographic capillary  
530 column system for the analysis of complex mixtures, *Chromatographia* 51 (2000) 108–120.
- 531 [4] Sz. Nyiredy, Z. Szücs, L. Szepeszy, Stationary phase optimized selectivity liquid  
532 chromatography: Basic possibilities of serially connected columns using the PRISMA  
533 principle, *J. Chromatogr. A* 1157 (2007) 122–130.
- 534 [5] K. Chen, F. Lynen, M. De Beer, L. Hitzel, P. Ferguson, M. Hanna-Brown, P. Sandra,  
535 Selectivity optimization in green chromatography by gradient stationary phase optimized  
536 selectivity liquid chromatography, *J. Chromatogr. A* 1217 (2010) 7222–7230.
- 537 [6] T. Alvarez-Segura, J.R. Torres-Lapasio, C. Ortiz-Bolsico, M.C. García-Alvarez-Coque,  
538 [Stationary phase modulation in liquid chromatography through the serial coupling of](#)  
539 [columns: A review, \*Anal. Chim. Acta\*, 923 \(2016\) 1-23.](#)
- 540 [7] T. Alvarez-Segura, C. Ortiz-Bolsico, J.R. Torres-Lapasio, M.C. Garcia-Alvarez-Coque,  
541 Serial versus parallel columns using isocratic elution: A comparison of multi-column  
542 approaches in mono-dimensional liquid chromatography, *J. Chromatogr. A* 1390 (2015) 95–  
543 102.
- 544 [8] G. Desmet, D. Clicq, P. Gzil, Geometry-independent plate height representation methods  
545 for the direct comparison of the kinetic performance of LC supports with a different size or  
546 morphology, *Anal. Chem.* 77 (2005) 4058–4070.
- 547 [9] D. Cabooter, F. Lestremau, F. Lynen, P. Sandra, G. Desmet, Kinetic plot method as a tool  
548 to design coupled column systems producing 100,000 theoretical plates in the shortest  
549 possible time, *J. Chromatogr. A* 1212 (2008) 23–24.

550 [10] U.D. Neue, M. Kele, Performance of idealized column structures under high pressure, J.  
551 Chromatogr. A 1149 (2007) 236-244.

552 [11] W.Th. Kok, U.A.Th. Brinkman, R.W. Frei, H.B. Hanekamp, F. Nooitgedacht, H. Poppe,  
553 Use of conventinal instrumentation with microbore column in high-performance liquid  
554 chromatography, J. Chromatogr. 237 (1982) 357-369.

555 [12] K. Broeckhoven, G. Desmet, Approximate transient and long time limit solutions for the  
556 band broadening induced by the thin sidewall-layer in liquid chromatography columns, J.  
557 Chromatogr. A 1172 (2007) 25-39.

558 [13] S. Fekete, K. Horvath, D. Guillarme, Influence of pressure and temperature on molar  
559 volume and retention properties of peptides in ultra-high pressure liquid chromatography, J.  
560 Chromatogr. A 1311 (2013) 65-71.

561 [14] F. Lestremau, A. de Villiers, F. Lynen, A. Cooper, R. Szucs, P. Sandra, High efficiency  
562 liquid chromatography on conventional columns and instrumentation by using temperature as  
563 a variable: Kinetic plots and experimental verification, J. Chromatogr. A 1138 (2007) 120-  
564 131.

565 [15] F. Lestremau, A. Cooper, R. Szucs, F. David, P. Sandra, High-efficiency liquid  
566 chromatography on conventional columns and instrumentation by using temperature as a  
567 variable: I. Experiments with 25 cm × 4.6 mm I.D., 5 µm ODS columns, J. Chromatogr. A  
568 1109 (2006) 191-196.

569 [16] D. Cabooter, G. Desmet, Performance limits and kinetic optimization of parallel and  
570 serially connected multi-column systems spanning a wide range of efficiencies for liquid  
571 chromatography, J. Chromatogr. A 1219 (2012) 114-127.

572 [17] A. Vaast, J. De Vos, K. Broeckhoven, M. Verstraeten, S. Eeltink, G. Desmet, Maximizing  
573 the peak capacity using coupled columns packed with 2.6 µm core-shell particles operated  
574 at 1200 bar, J. Chromatogr. A 1256 (2012) 72-79.

575 [18] U.D. Neue, Peak capacity in unidimensional chromatography, J. Chromatogr. A 1184  
576 (2008) 107-130.

577 [19] S. Fekete, J.L. Veuthey, D. Guillarme, Comparison of the most recent chromatographic  
578 approaches applied for fast and high resolution separations: Theory and practice, J.  
579 Chromatogr. A 1408 (2015) 1-14.

580 [20] S. Fekete, M.W. Dong, T. Zhang, D. Guillarme, High resolution reversed phase analysis  
581 of recombinant monoclonal antibodies by ultra-high pressure liquid chromatography column  
582 coupling, J. Pharm. Biomed. Anal. 83 (2013) 273-278.

583 [21] D. Guillarme, E. Grata, G. Glauser, J.L. Wolfender, J.L. Veuthey, S. Rudaz, Some  
584 solutions to obtain very efficient separations in isocratic and gradient modes using small  
585 particles size and ultra-high pressure, J. Chromatogr. A 1216 (2009) 3232-3243.

586 [22] S. Fekete, A. Beck, D. Guillarme, Characterization of cation exchanger stationary  
587 phases applied for the separations of therapeutic monoclonal antibodies, J. Pharm. Biomed.  
588 Anal. 111 (2015) 169-176.

589 [23] A.G.G. Perrenoud, C. Hamman, M. Goel, J.L. Veuthey, D. Guillarme, S. Fekete,  
590 Maximizing kinetic performance in supercritical fluid chromatography using state-of-the-art  
591 instruments, J. Chromatogr. A 1314 (2013) 288-297.

592 [24] N.C.P. Albuquerque, J.V. Matos, A.R.M. Oliveira, In-line coupling of an achiral-chiral  
593 column to investigate the enantioselective in vitro metabolism of the pesticide Fenamiphos  
594 by human liver microsomes, J. Chromatogr. A 1467 (2016) 326-334.

595 [25] R. Eksteen, H.G. Barth, B. Kempf, The effect of sec column arrangement of different  
596 pore sizes on resolution and molecular weight measurements, LCGC North America, 29  
597 (2011) 668–671.

598 [26] A. Jones, S. Pravadali-Cekic, G.R. Dennis, R.A. Shalliker, Post column derivatisation  
599 analyses review. Is post-column derivatisation incompatible with modern HPLC columns?,  
600 Anal. Chim. Acta, 889 (2015) 58-70.

601 [27] M. Javanbakht, M.M. Moein, B. Akbari-adergani, On-line clean-up and determination of  
602 tramadol in human plasma and urine samples using molecularly imprinted monolithic column  
603 coupling with HPLC, J. Chromatogr. B, 911 (2012) 49-54.

604 [28] S. Schweiger, S. Hinterberger, A. Jungbauer, Column-to-column packing variation of  
605 disposable pre-packed columns for protein chromatography, *J. Chromatogr. A*, 1527 (2017)  
606 70-79.

607 [29] L.R. Snyder, J.W. Dolan, High-performance gradient elution: The practical application of  
608 the linear solvent strength model, John Wiley & Sons, Inc. 2007

609 [30] B. Bobaly, V. D'Atri, A. Goyon, O. Colas, A. Beck, S. Fekete, D. Guillarme, Protocols for  
610 the analytical characterization of therapeutic monoclonal antibodies. II – Enzymatic and  
611 chemical sample preparation, *J. Chromatogr. B* 1060 (2017) 325-335.

612

613

614 Table 1.

615

column	L (mm)	N							
		methylparaben		ethylparaben		propylparaben		butylparaben	
		measured	predicted	measured	predicted	measured	predicted	measured	predicted
A	150	15111	-	14911	-	14763	-	15070	-
B	100	6066	-	6329	-	6512	-	6889	-
C	75	11509	-	12046	-	12478	-	12681	-
A+B	250	19388	19920	19792	20233	19863	20427	20956	21225
A+C	225	24744	25598	24955	25621	25599	25635	25902	26414
B+C	175	14406	14329	15301	14961	15921	15417	16440	16160
A+B+C	325	27857	29128	28757	29704	29256	30088	30690	31174

616

617 Table 2.

618

column	L (mm)	peak 1		peak 11		Rs crit 9.10	peak capacity
		$w_{1/2}$	$w_{1/2}$	$w_{1/2}$	$w_{1/2}$		
		measured (min)	predicted (min)	measured (min)	predicted (min)		
A	150	0.0571	-	0.0715	-	0.69	134
B	100	0.0666	-	0.0771	-	0.55	83
C	75	0.0375	-	0.0399	-	0.57	119
B+A	250	0.0909	0.0993	0.1031	0.1162	0.88	144
C+A	225	0.075	0.0698	0.0838	0.0870	0.99	159
C+B	175	0.0852	0.0861	0.0964	0.0994	0.57	110
A+B+C	325	0.1054	0.0957	0.1098	0.1084	1.00	167

619

620

621 Table 3.

622

column	L (mm)	peak 1		peak 2		peak 3		peak capacity
		$w_{1/2}$	$w_{1/2}$	$w_{1/2}$	$w_{1/2}$	$w_{1/2}$	$w_{1/2}$	
		measured (min)	predicted (min)	measured (min)	predicted (min)	measured (min)	predicted (min)	
D	150	0.0697	-	0.0703	-	0.0781	-	240
E	150	0.0592	-	0.0559	-	0.0525	-	312
D + E	300	0.0918	0.0857	0.0849	0.0819	0.088	0.0797	388
E + D	300	0.0923	0.0968	0.095	0.0971	0.0966	0.1066	362

623

624

625 **Figure captions**

626

627 Figure 1.  $N_{app}/N_{sum}$  (relative apparent efficiency of the coupled system) as a function of  $N_1/N_2$   
628 (ratio of individual column efficiency) for various column length ratios ( $L_1/L_2 = 0.75, 1, 1.5$  and  
629 2).

630

631 Figure 2. Experimentally obtained chromatograms of a mixture of uracil and 4 parabens on  
632 columns A, B and C and on serially connected columns A+B+C in isocratic mode. The  
633 mobile phase was composed of 55 : 45 v/v water : acetonitrile. Experiments were performed  
634 at a flow rate of 1 mL/min at ambient temperature. Detection was carried out at 254 nm (40  
635 Hz), the injection volume was 5  $\mu$ L. Peaks: uracil ( $t_0$ ), methylparaben (1), ethylparaben (2),  
636 propylparaben (3) and butylparaben (4).

637

638 Figure 3.  $N_{app}/N_1$  (apparent efficiency compared to the first column) as a function of  $N_1/N_2$   
639 (ratio of individual column efficiency) for various column length ratios ( $L_1/L_2 = 0.2, 1, \text{ and } 2$ ).

640

641 Figure 4. The evolution of peak variance ( $\sigma_z$ ) along the column ( $z$ ) for a system composed of  
642 two columns coupled in series. Three cases **named A to C** are reported, corresponding to  
643 different segment lengths and gradient steepness, considering  $H = 10 \mu\text{m}$  and  $40 \mu\text{m}$ . Please  
644 note that time based peak width as a practical measure of band broadening can be obtained  
645 at the total length by  $= \frac{\sigma_z(L)}{u_0}$ .

646

647 Figure 5. Experimental chromatograms of cannabinoids mixture on columns A, B and C and  
648 on serially connected combinations in gradient mode. Linear gradients were run from 45 to  
649 100 %B at 1 mL/min and ambient temperature. The gradient time ( $t_G$ ) over column length (L)  
650 ratio was kept constant ( $t_G/L=1 \text{ min/cm}$ ) when running gradients on different column lengths.  
651 Detection was carried out at 254 nm (40 Hz), and injection volume was 10  $\mu$ L.

652

653 Figure 6. Experimental chromatograms of HSA tryptic digest on columns D and E and on  
654 serially connected "D+E" and "E+D" combinations in gradient mode. Linear gradients were  
655 run from 10 to 70 %B at 0.3 mL/min and 50 °C. The gradient time ( $t_G$ ) over column length (L)  
656 ratio was kept constant ( $t_G/L=2 \text{ min/cm}$ ) when running gradients on different column lengths.  
657 Detection was carried out at 280 nm as fluorescence excitation and 350 nm as fluorescence  
658 emission wavelengths, and injection volume was 5  $\mu$ L.

659

660

661 **Table captions**

662

663 Table 1. Measured and predicted plate numbers for parabens in isocratic mode on three  
664 individual columns and on their different combinations. (Predictions are based on eq. 18 for  
665 two columns and 12 for three columns.)

666

667 Table 2. Measured and predicted peak widths for cannabinoids in gradient elution mode on  
668 three individual columns and on their different combinations. The obtained critical resolution  
669 and peak capacity are also shown. (Predictions are based on eq. 47-49.)

670

671 Table 3. Measured and predicted peak widths for peptides obtained in gradient elution mode  
672 on two individual columns and on their combinations. The obtained peak capacity is also  
673 indicated. (Predictions are based on eq. 47-49.)

674

Figure

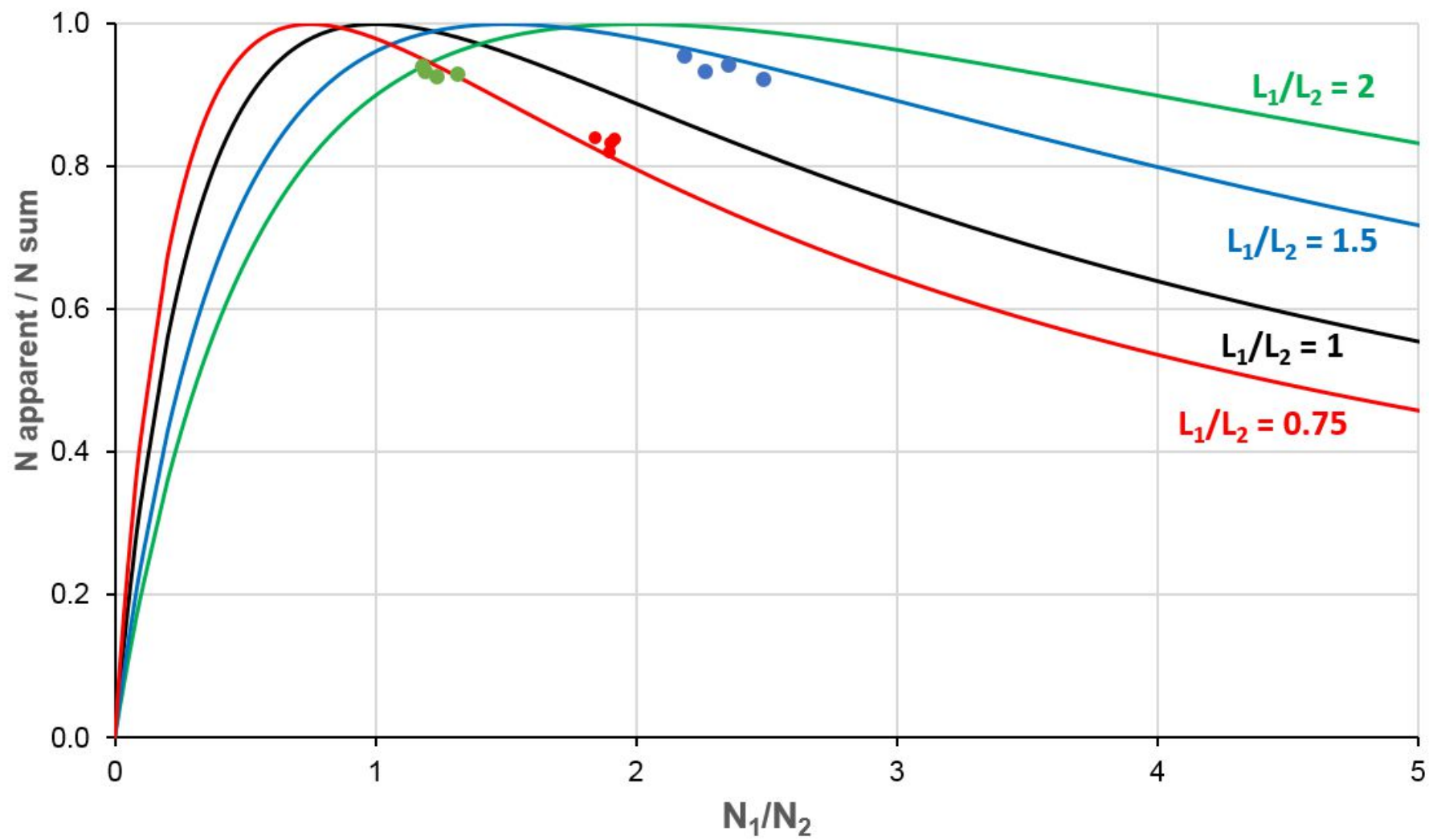


Figure 1

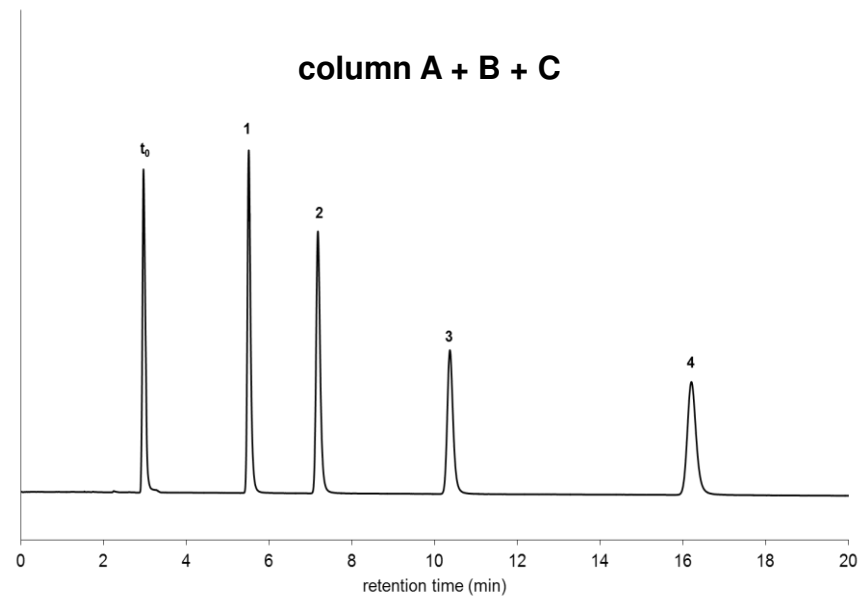
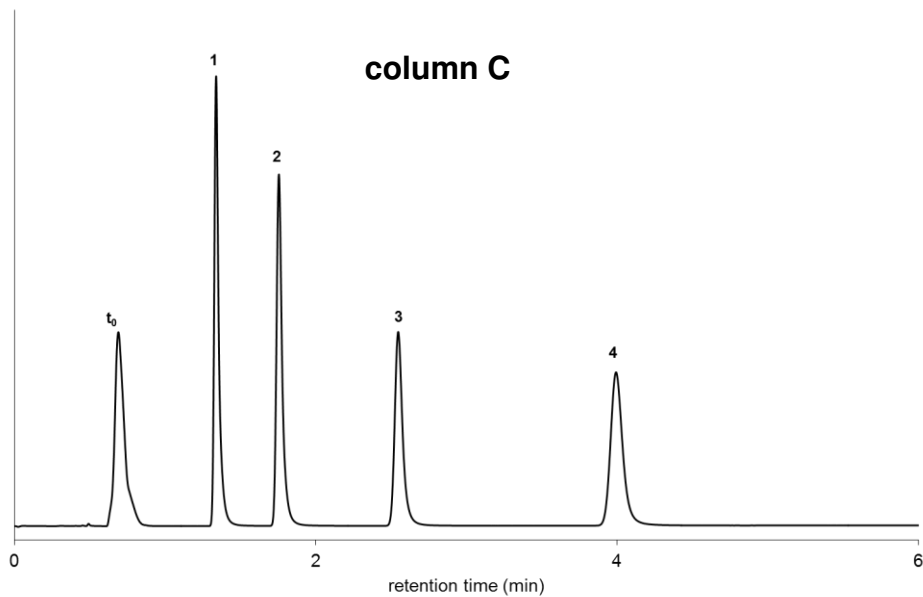
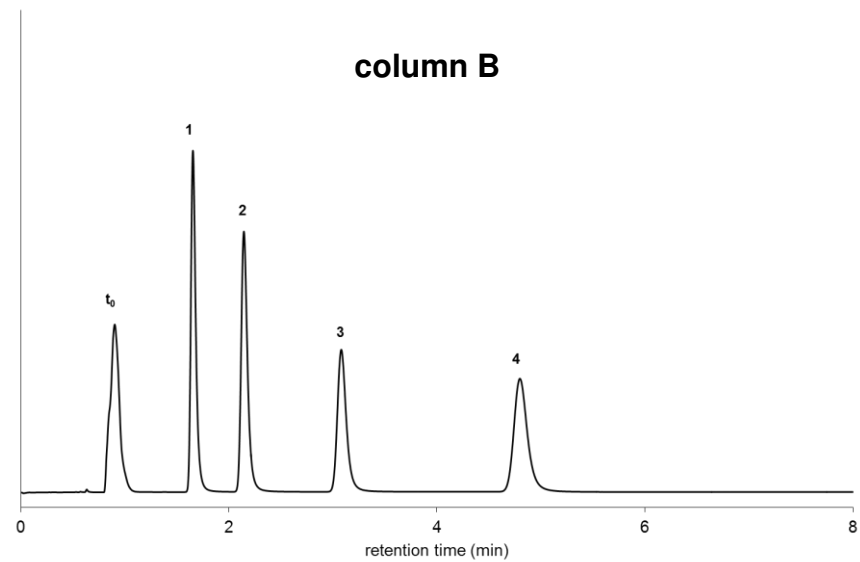
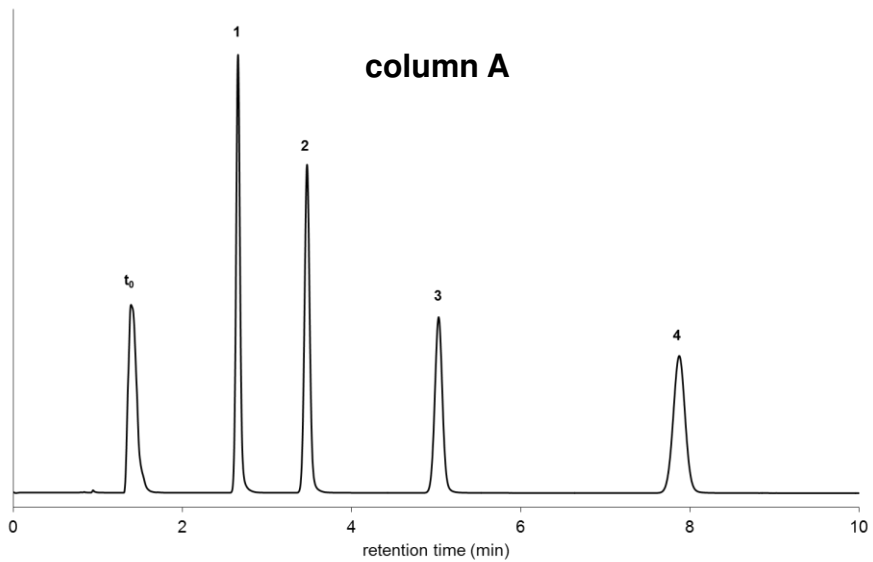


Figure 2

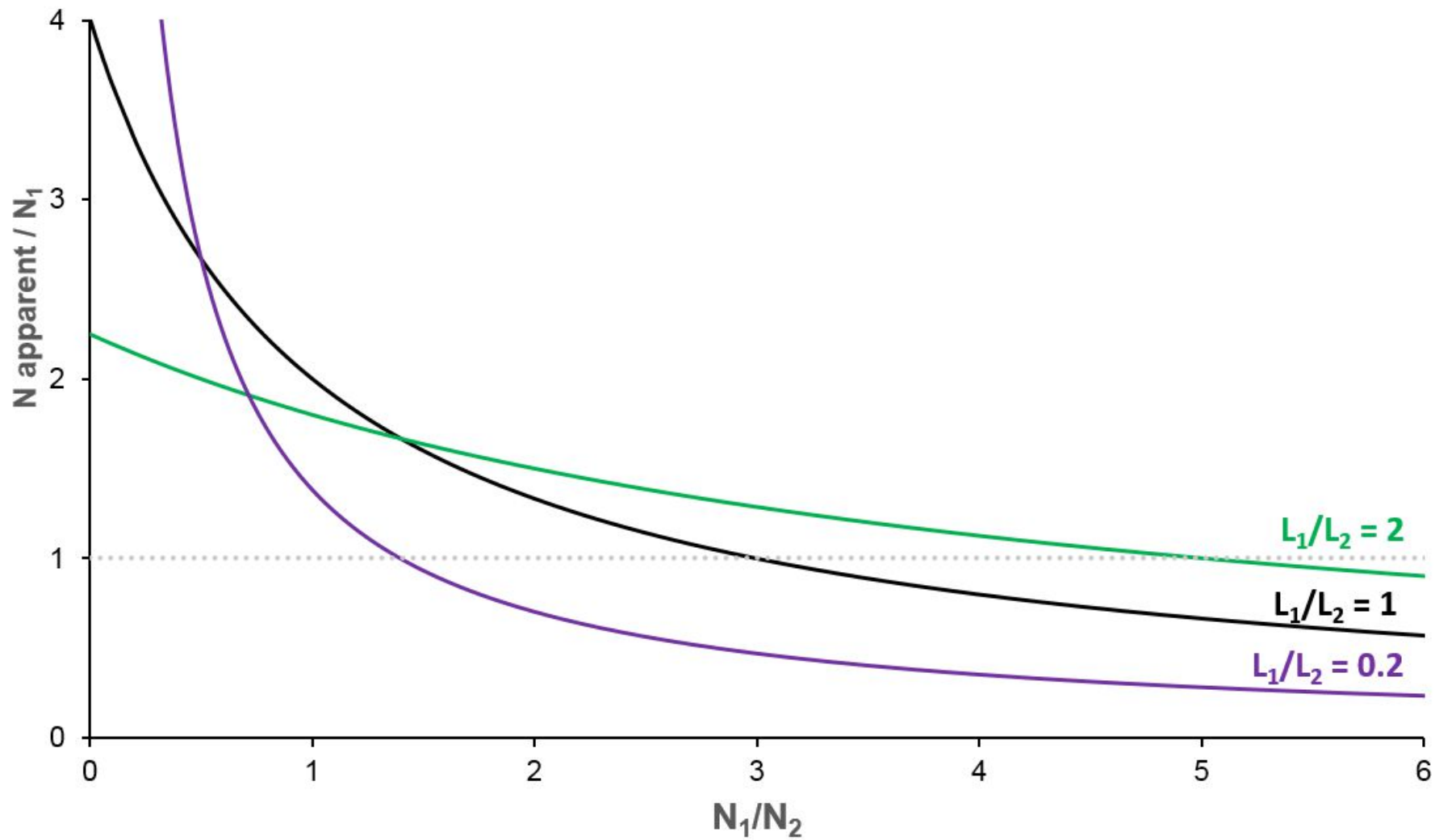


Figure 3

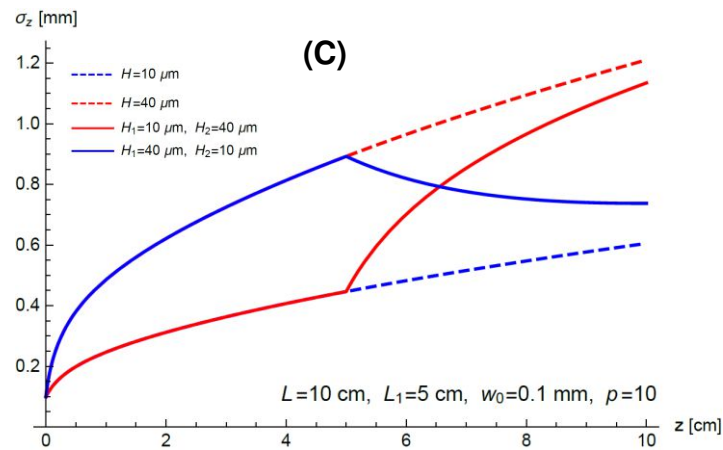
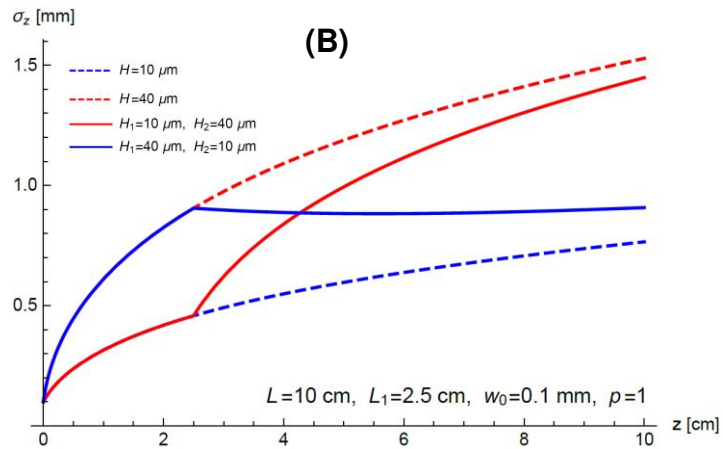
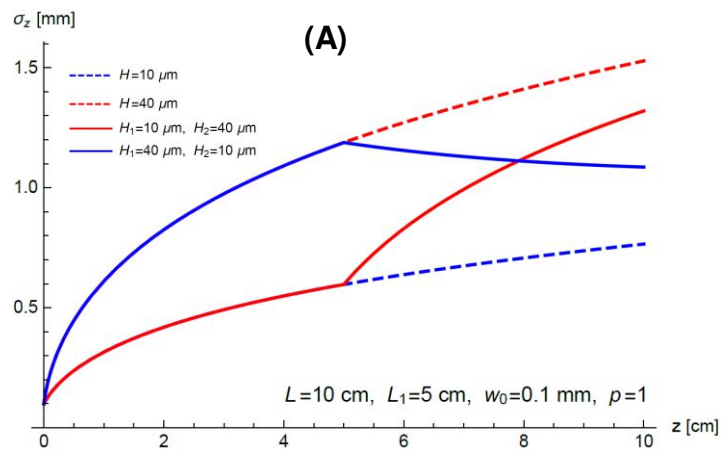


Figure 4

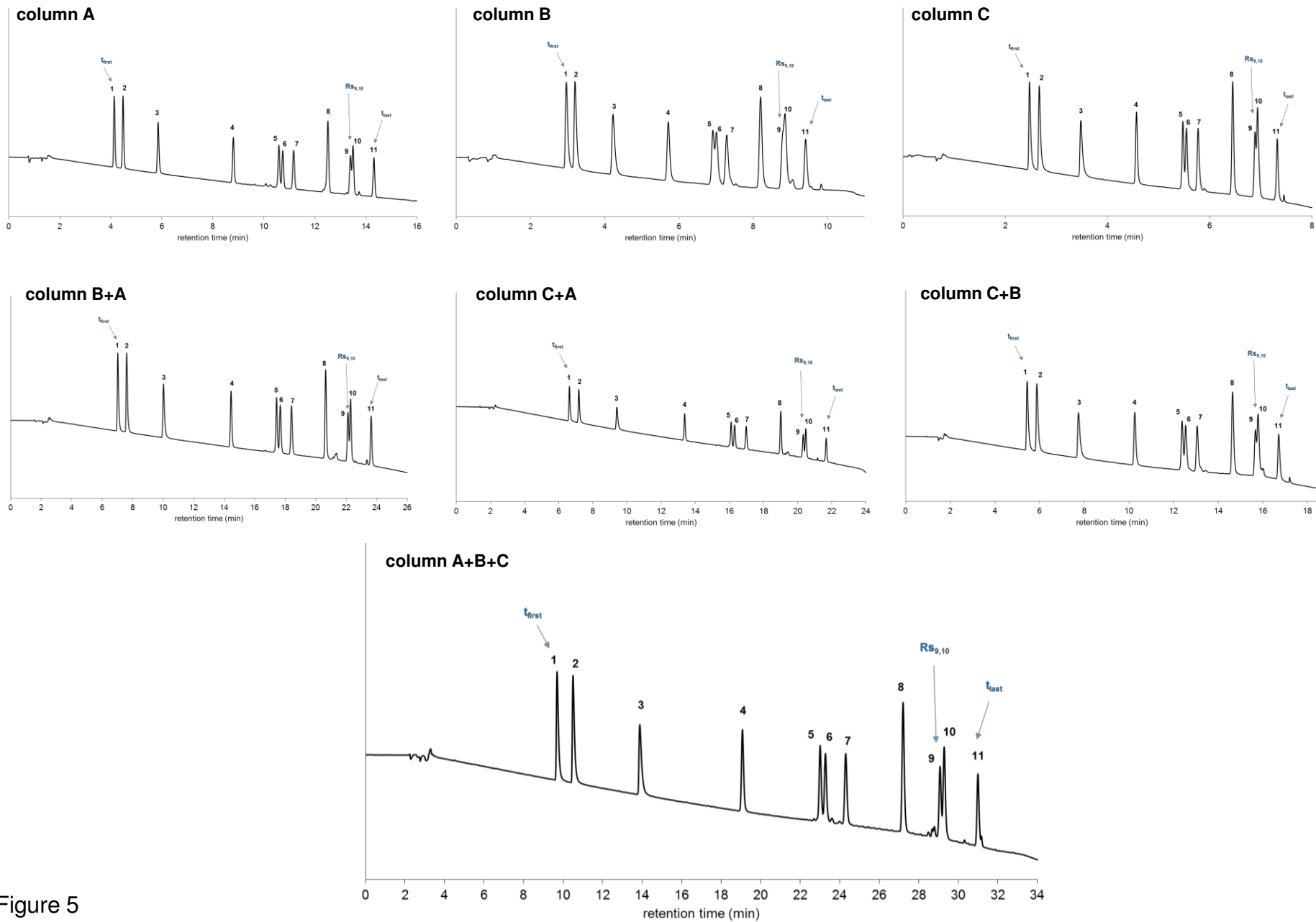
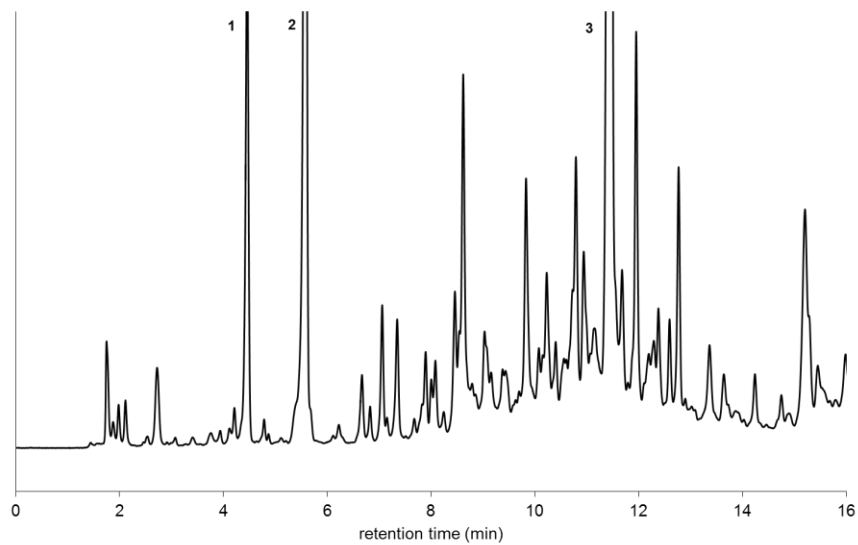
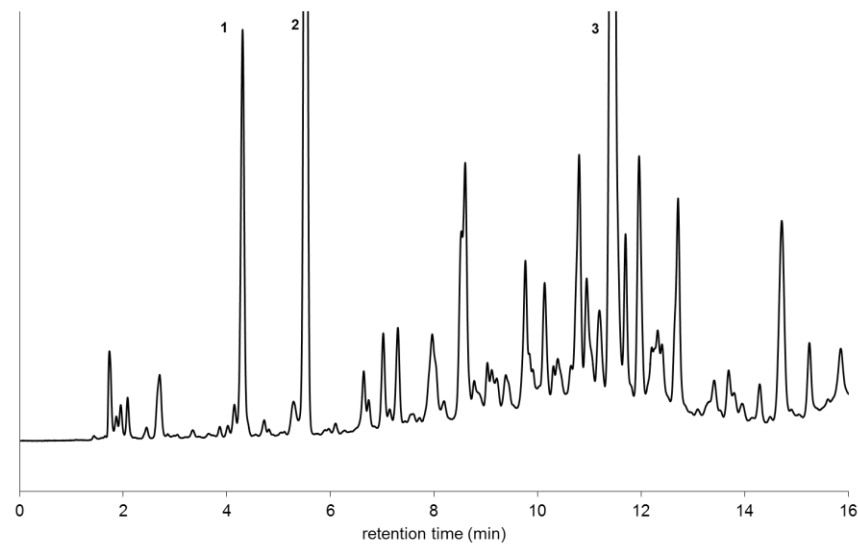


Figure 5

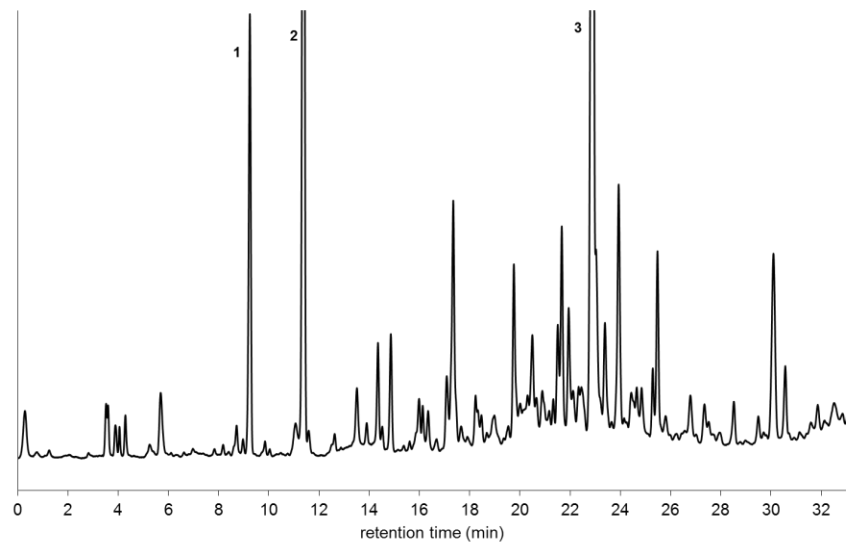
**column D**



**column E**



**column D + E**



**column E + D**

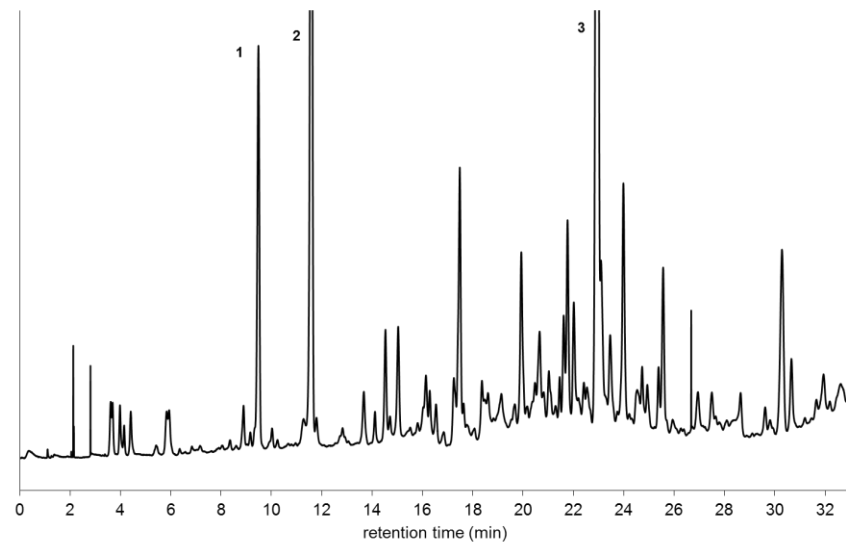


Figure 6